Section 4

Parameterization of atmospheric and surface processes, effects of different physical parameterizations.

Numerical Simulation of Potential Impact of Aerosols on Heavy Snowfall Events Associated with Japan-Sea Polar-Airmass Convergence Zone

Kentaro Araki[1]

1: Meteorological Research Institute, Tsukuba, Ibaraki, Japan

e-mail: araki@mri-jma.go.jp

1. Introduction

Aerosols play a key role not only in the earth climate, but also in short-term precipitation phenomena, working as cloud condensation nuclei (CCNs) and ice nuclei (INs). Although recent studies have suggested aerosol indirect effects on convective clouds and mesoscale convective systems such as invigoration process by CCNs, uncertainties still remain especially in the aerosol properties of INs and their effects on cloud and precipitation systems (Araki and Sato, 2018). For the heavy snowfall events in the Pacific regions in Japan, it is indicated that the aerosol indirect effect by INs considerably affected snowfall amounts and distribution (Araki and Murakami, 2015; Araki, 2016). On the other hand, it is known that the Japan-sea Polar-airmass Convergence Zone (JPCZ) sometimes brings extreme heavy snowfall in the areas on the Japan Sea side compared with the areas in the Pacific side in winter. In this study, we investigated the potential impacts of aerosol indirect effects by CCNs and INs on the forecast for the heavy snowfall events in the areas in the Japan Sea side associated with the JPCZ.

2. Model settings of sensitivity experiments

Numerical simulations were performed by the Japan Meteorological Agency (JMA) Non-Hydrostatic Model (NHM) with a domain of 2,400x2,000 km covering Japan and a horizontal grid spacing of 2 km. The initial and boundary conditions were provided from the 6-hourly JRA-55 reanalysis data and the models were run from 00 UTC on 3 to 00 UTC on 8 February 2018. A convection parameterization scheme was not used and a bulk cloud microphysics scheme with 2-moment cloud water, cloud ice, snow, and graupel was used in a control run (CNTL). As sensitivity experiments on CCNs, experiments with changing a coefficient of number concentration of cloud droplets in the formula of cloud condensation nucleation by factors of 0.1 (CN01) and 10 (CN10) were performed. Focusing on the aerosol indirect effect by INs, we also performed experiments with changing coefficients in the formulas of deposition/condensation-freezing-mode ice nucleation (Meyers, 1992) and immersion-freezing-mode ice nucleation (Bigg, 1955) by factors of 0.1 (IN01) and 10 (IN10). In addition, combining these settings, we conducted two sensitivity experiments assuming clean (CIN01) and dirty (CIN10) environments. The other setups in each experiment were the same as those used in Saito et al. (2006).

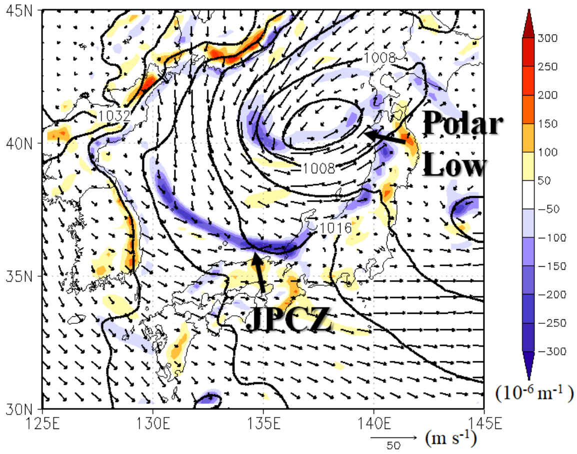

Figure 1. Environmental conditions at 00 UTC on 7 February 2018 obtained from the JMA global analysis. Horizontal distributions of horizontal divergence at 950 hPa (shaded) and sea level pressure (contour).

3. Potential effect of CCNs and INs on a heavy snowfall event associated with the JPCZ

From 3 to 7 February 2018, a polar low had maintained over the Japan Sea under the unstable atmospheric conditions with upper cold air flow (Fig. 1). The JPCZ clearly formed on 4, and had been sustained until 7 February. Convective clouds associated with the JPCZ brought heavy snowfall in the areas in the Japan Sea side, the total snowfall and precipitation amounts in Fukui respectively reached 143 cm and 169.5 mm from 00 UTC on 3 to 00 UTC on 8 February.

The radar analysis, results of simulated precipitation in CNTL, and the differences from CNTL for each experiment are shown in Fig. 2. From the comparison with radar analysis, the CNTL successfully reproduced heavy snowfall associated with the JPCZ in the land areas including Fukui. In the sensitivity experiments, there were the differences of snowfall areas with precipitation amount of 10–20 mm from CNTL because of the differences of the representations for the location of convective clouds. Although the CN01 and CN10 had the similar difference from the CNTL, there were significant differences with respect to the precipitation amounts (intensity) in the other experiments. From the results that the differences of precipitation amount over the Japan Sea from the CNTL for IN01, IN10, CIN01, and CIN10 were larger than those for CN01 and CN10, it was suggested that the INs were highly sensitive to the formation and development of convective clouds associated with the JPCZ. Table 1 shows the maximum, minimum, and averaged differences of precipitation amounts from the CNTL for each experiment in the heavy snowfall areas including Fukui. The absolute values of maximum and minimum differences for IN01, IN10, CIN01, and CIN10 were about 1.5 to 2 times those for CN01 and CN10. It was also found that precipitation amount increased in the heavy snowfall areas including Fukui in IN10 and CIN10 compared with the CNTL, and opposite features were found in IN01 and CIN01. There were the same characteristics of precipitation amount for all domains of the simulation.

From these results, it is indicated that the quantitative forecast of precipitation amount is sensitive to the aerosol effect by CCNs and INs, and that the effect of INs would be more significant than that of CCNs in this case. It is desired that the parameterization of CCNs and INs in mesoscale models for the short-term forecast should be improved in the future.

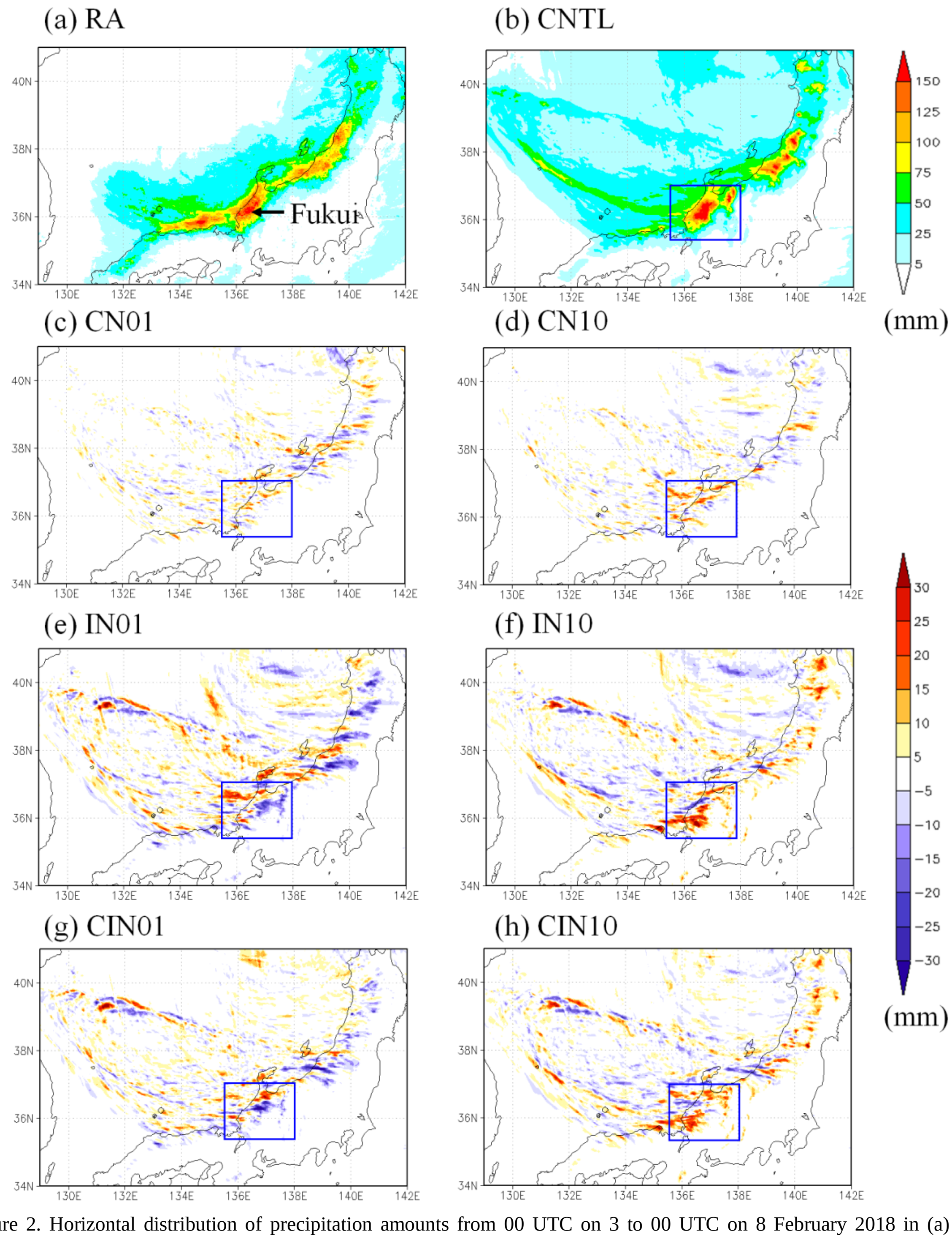

Figure 2. Horizontal distribution of precipitation amounts from 00 UTC on 3 to 00 UTC on 8 February 2018 in (a) radar analysis (RA), (b) CNTL, and (c)-(h) the differences from CNTL for each experiment.

Table 1. Differences of simulated precipitation amounts from 00 UTC on 3 to 00 UTC on 8 February 2018 in each experiment from CNTL. Maximum, minimum, and averaged values (mm) in the area of blue rectangular in Fig. 2 (b)-(h) are shown.

(mm)	CN01	CN10	IN01	IN10	CIN01	CIN10
Max	20.59	26.67	30.50	44.29	33.52	33.40
Min	-20.17	-21.23	-40.09	-32.48	-49.62	-26.40
Ave	0.59	1.68	-1.65	3.01	-1.24	2.81

References:

Araki, K., 2016: Influence of cloud microphysics scheme and ice nuclei on forecasting a heavy snowfall event in Japan associated with the "South-Coast Cyclones". *CAS/JSC WGNE Research Activities in Atmospheric and Oceanic Modelling*, **46**, 4.03–4.04.

Araki, K., and M. Murakami, 2015: Numerical simulation of heavy snowfall and the potential role of ice nuclei in cloud formation and precipitation development. *CAS/JSC WGNE Research Activities in Atmospheric and Oceanic Modelling*, **45**, 4.03–4.04.

Araki, K., and Y. Sato, 2018: Review of numerical simulation studies of aerosol impacts on clouds and precipitation. *Earozoru Kenkyu*, **33**, 152-161.

How Robust are Neural Network Emulations of Model Physics with Respect to Changes in Model Phase Space?

Alexei Belochitski[1,2], Vladimir Krasnopolsky[2]

[1]IMSG, [2]NOAA/NWS/NCEP/EMC

email: **alexei.a.belochitski@noaa.gov**

1 Neural Network Emulations of Model Physics

One of the main difficulties in developing and implementing high-resolution environmental models is the complexity of the physical processes involved. For example, the calculation of radiative transfer in a GCM often takes a significant part of the total model computation and is necessarily a trade-off between accuracy and computational efficiency. Very accurate methods exist, such as line-by-line procedures, that are, however, too computationally prohibitive to be used in GCMs, and, therefore, radiative transfer is parameterized, for example, by the correlated-k method. Nevertheless, even further computational cost reductions are needed and thus radiation calculations are usually made at lower temporal and/or spatial resolutions than the rest of the model followed by an interpolation of the results to an original finer grid. Such approaches reduce the horizontal, or vertical, or temporal variability of radiation fields and their consistency with other parts of model physics and with dynamics, which may, in turn, negatively affect the accuracy of climate simulations and weather prediction. For example, in the pre-operational version of NCEP FV3 GFS radiative transfer calculations are performed once per model hour and are interpolated on the much finer physical time step of 225 s when the rest of model's physical parameterizations are called. One approach addressing these issues is based on using neural networks to "emulate" existing physical parameterizations.

Any parameterization of model physics is a mapping (continuous or almost continuous) between two vectors: a vector of the input variables of parameterization and a vector of its output variables. A neural network (NN) is a generic approximation for any continuous or almost continuous mapping given by a set of its input and output records. Existence of the approximation is guaranteed, and its error bound is independent of the dimensionality of the mapping (e.g., Krasnopolsky (2013)). NNs are very accurate, fast, and convenient statistical models able to approximate numerical model components, which in essence are complex nonlinear input/output relationships. Finding the analytical expression for the approximation (or "training" the NN) is a complicated and time consuming nonlinear optimization procedure; however, training should be done only once for a particular application.

An NN emulation of a model physics parameterization is a functional imitation of this parameterization in the sense that the results of model calculations with the original parameterization and with its NN emulation are physically identical. It is accomplished by using the data for NN training simulated by running the original model with the original parameterization, which allows to achieve a very high accuracy of approximation because simulated data are free of the problems typical of empirical data.

Previous work has demonstrated the practical possibility of using highly efficient NN emulations for the full (long- and short-wave) model radiation for decadal climate simulations in a coupled climate model with prescribed time dependent CO_2 and aerosols (NCEP CFS T126L64) by Krasnopolsky et al. (2010), and a high resolution short- to medium- range weather forecasting model (NCEP GFS T574L64) by Krasnopolsky et al. (2012). A very high accuracy and up to two orders of magnitude increase in speed as compared to the original parameterization for both NCEP CFS and GFS full radiation has been achieved. The systematic errors introduced by NN emulations of full model radiation are negligible and do not accumulate during the decadal model simulation. The random errors of NN emulations are also small. Almost identical results have been obtained for the parallel multi-decadal climate runs of the models using the NN and the original parameterization, and in limited testing in the medium-range forecasting mode.

The mapping approximated by an NN is defined not only by the parameterization that is being emulated, but by the entirety of the atmospheric model environment: the dynamical core, the suit of physical parameterizations, and the set of configuration parameters for both. Once any of these is modified, the set of possible model states is modified as well, possibly now including states that were absent in the NN's training data set. It is natural to ask how much of a change in the model's phase space can a statistical model like the NN tolerate? The answer will also provide an insight into how an NN emulation might fare under a change in boundary conditions, such as a change in greenhouse gas concentrations.

2 FV3 GFS experiments with 2011 GFS LW and SW NN Radiation

NN emulations of the LW and SW radiative transfer parameterizations, originally developed within the framework of the 2011 versions of GFS and CFS, were incorporated into the preoperational version of FV3 GFS. They can be used in place of the default RRTMG LW v4.82 and SW v3.8.

FV3 GFS differs from the 2011 version of GFS in a number of ways, most significant of which are the new dynamical core (FV3), microphysical parameterization (GFDL MP), PBL scheme (Hybrid EDMF), and a different set of values of tuning parameters. The most consequential change appears to be the replacement of the Zhao-Carr microphysics with the GFDL scheme. The reasons for this are twofold. The most important is a design choice made during development of the LW NN. Inputs to the RRTMG LW parameterization include, among others, vertical profiles of temperature, specific humidity, cloud fraction, liquid water path, ice water path, effective radius of liquid droplets, and effective radius of ice crystals. The last five profiles are calculated by the microphysical parameterization from the first two and are correlated with one another. Since profiles of specific humidity and temperature are already inputs to the LW NN, inclusion of only one cloud-related profile (cloud fraction) allows the NN to emulate the remaining four. In effect, LW NN emulates not only the radiative transfer parameterization, but also calculations of cloud properties by microphysics.

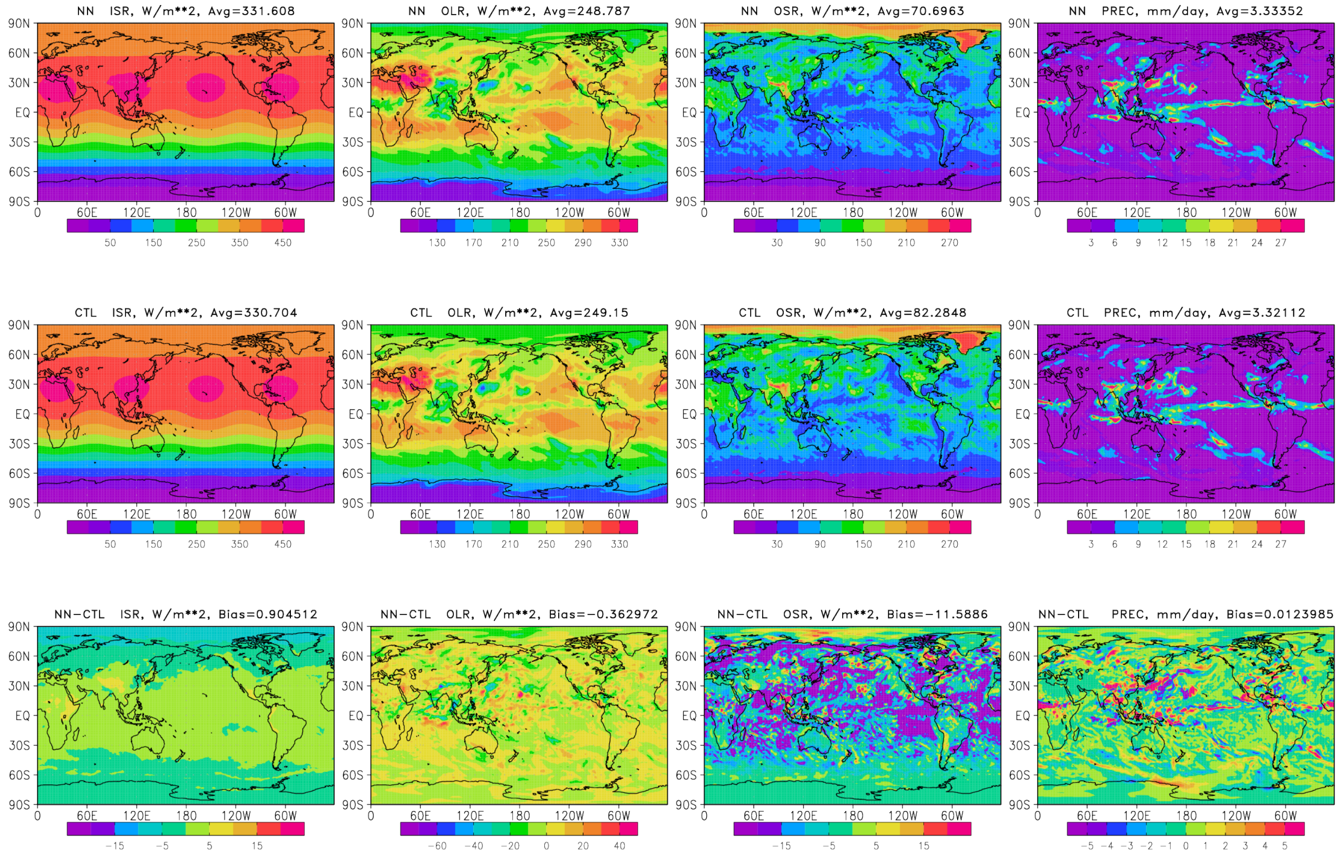

(a) Incoming SW , W/m^2 (b) OLR, W/m^2 (c) OSR, W/m^2 (d) Precipitation rate, mm/day

Figure 1: Full NN radiation vs control, Zhao-Carr MP, day 3-10 average of a C96 forecast initialized at 00Z on 8/1/17.

Consequently, when the microphysical parameterization is replaced, the internal representation of cloud properties in the NN is no longer consistent with the rest of the model.

Another possible contributing factor is that the change in microphysical parameterization leads to the near doubling of the model's prognostic variables from 7 to 12, and to the proportional increase in dimensionality of the physical phase space of the model. As a result, the set of possible model states in FV3 GFS is very different from a mathematical standpoint from the 2011 model version. Even though the vectors of inputs to the radiative transfer parameterizations remain the same, they are obtained by mapping from a very different mathematical object, potentially increasing the probability that a given input vector lies outside of the NNs original training data set.

These fundamental physical and mathematical inconsistencies between the 2011 GFS NN and FV3 GFS environment have led us to replace the GFDL microphysics with the Zhao-Carr scheme that was used to generate the 2011 NN training set. It is possible or even likely that the choice of tuning parameters in Zhao-Carr microphysics is different in FV3 GFS then what was used in the 2011 model (and what is implicitly built in into the NN). Therefore, we tune the value of the dimensionless coefficient of autoconversion of ice to snow, doubling it from 8e-4 to 16e-4 in the NN run, but keep it unchanged in the control.

Figure 1 shows averages over days 3-10 of a 10-day forecast initialized at 00Z on 08/01/17 at C96L64 resolution ($\sim$ 100 km horizontal grid size) produced by the current pre-operational FV3 GFS with Zhao-Carr MP (control) and the same model using both LW and SW NNs. The largest discrepancy is in outgoing SW at TOA (Fig. 1c), while discrepancies in incoming SW (Fig. 1a) and outgoing LW (Fig. 1b) at TOA are within observational uncertainties, as are the rest of radiative fluxes (not shown). Precipitation (Fig. 1d) is to the first order determined by the atmospheric energy balance, and differs only by 0.01 mm/day between the two runs. Overall, these results indicate significant robustness in the NN emulations with respect to the changes in the model, at least in the limited number of experiments. The NN performs like a plausible physical parameterization, tolerating the aforementioned significant changes in the model, provided that fundamental assumptions about the host model (like cloud properties) made during NN design did not change significantly.

The next step in our project is to generate the NN training data set using the FV3 GFS (including GFDL MP and all other upgrades) with the goal of calling NN emulations of the radiative transfer parameterizations at every physical time step.

References

Krasnopolsky, V., A. A. Belochitski, Y.-T. Hou, S. Lord, and F. Yang: 2012, Accurate and fast neural network emulations of long and short wave radiation for the NCEP Global Forecast System model. *NCEP Office Note*, **471**, Camp Springs, MD.

Krasnopolsky, V., M. Fox-Rabinovitz, Y.-T. Hou, S. Lord, and A. A. Belochitski: 2010, Accurate and fast neural network emulations of model radiation for the NCEP coupled climate forecast system: Climate simulations and seasonal predictions. *Mon. Wea. Rev.*, **138**, 1822–1842.

Krasnopolsky, V. M.: 2013, *The Application of Neural Networks in the Earth System Sciences: Neural Network Emulations for Complex Multidimensional Mappings*. Springer Publishing Company, Incorporated.

Simplified High Order Closure in FV3 GFS

Alexei Belochitski[1,2], Steven Krueger[3], Shrinivas Moorthi[2], Peter Bogenschutz[4], Anning Cheng[1,2]

[1]IMSG, [2]NOAA/NWS/NCEP/EMC, [3]U. of Utah, [4]DOE/LLNL

email: **alexei.a.belochitski@noaa.gov**

1 Introduction

One approach to high order turbulence closure is to assume a functional form of the subgrid probability density distribution of relevant model variables, determine parameters of this distribution using its lower order moments that the model explicitly prognoses and/or diagnoses, and then use the distribution to infer the unknown higher order moments necessary to close the model. Ideally, the PDF should be flexible enough to account for all the regimes of subgrid scale (SGS) moist turbulence in the atmosphere as well as transitions from one regime to another, yet sufficiently simple so the model only needs to predict a computationally feasible number of moments. A joint PDF, $P(w,\theta_l,q_t)$, trivariate in subgrid vertical velocity, w, liquid water potential temperature, θ_l, and total specific cloud condensate content, q_t, based on a double Gaussian function in each variable was demonstrated to be a good fit for the data observed by aircraft and simulated by LES with a 100 m horizontal resolution for stratocumulus, as well as in trade wind and continental cumulus cases by Larson et al. (2002). This analysis was extended with similar results for CRM data with horizontal resolutions up to 25 km for a clear convective boundary layer, non-precipitating and precipitating marine and continental shallow cumulus, marine stratocumulus, and transition from stratocumulus to cumulus by Bogenschutz et al. (2010).

The trivariate double Gaussian PDF has 19 parameters. However, the complete set of 19 first, second, and third order moments does not uniquely determine parameters of this PDF. If some parameters of the PDF are expressed in terms of others, then the number of independent parameters can be reduced and the functional form of the PDF effectively modified to potentially be uniquely realizable in terms of its moments. One such simplification, the Analytic Double Gaussian 1 (ADG1), has 13 parameters that are uniquely determined by the following 10 moments: $\overline{w}$, $\overline{\theta_l}$, $\overline{q_t}$, $\overline{w'^2}$, $\overline{\theta_l'^2}$, $\overline{q_t'^2}$, $\overline{w'\theta_l'}$, $\overline{w'q_t'}$, $\overline{\theta_l'q_t'}$, $\overline{w'^3}$. Note that only one third order moment, $\overline{w'^3}$, is needed to recover the PDF.

An additional advantage of using a PDF in the form of $P(w,\theta_l,q_t)$ is that it can be integrated over the saturated part of the $\theta_l - q_t$ plane to obtain the cloud fraction and amount of total condensate. Moreover, SGS buoyancy flux can be computed from the same PDF. Overall, the PDF provides a self-consistent way of deriving the higher order moments of SGS turbulence along with properties of SGS cloudiness.

2 Simplified High Order Closure

Cheng et al. (2010) used a CRM with a $1\frac{1}{2}$-order TKE-based closure that calculated turbulent diffusion coefficients from SGS TKE following the Smagorinsky-Lilly approach, and diagnosed the SGS fluxes $\overline{w'\theta_l'}$ and $\overline{w'q_t'}$ using a simple downgradient diffusion method. They found that both the TKE and diagnosed SGS fluxes were too weak compared to a corresponding LES simulation. However, when they replaced the TKE calculation in the CRM with TKE computed in the corresponding LES run, they found that the diagnosed SGS fluxes along with resolved circulation were drastically improved.

Bogenschutz and Krueger (2013) conjectured that as long as the right amount of TKE is predicted, then *all* second order moments, $\overline{\theta_l'^2}, \overline{q_t'^2}, \overline{w'\theta_l'}, \overline{w'q_t'}, \overline{\theta_l'q_t'}$, can be predicted correctly using the downgradient diffusion method ($\overline{w'^2}$ can be inferred from TKE). They used a diagnostic expression for $\overline{w'^3}$ from Canuto et al. (2001) that is dependent on the values of lower order moments, and coupled a prognostic TKE equation in another $1\frac{1}{2}$-order closure CRM to ADG1, calculating SGS PDF's parameters using the diagnostic approach outlined above. The SGS PDF was used to calculate a SGS buoyancy flux term for the TKE equation and as a condensation/cloud fraction scheme for the CRM. They called this approach Simplified High Order Closure (SHOC).

The prognostic TKE equation is the "backbone" of SHOC, as the success or failure of the scheme hinges on an accurate calculation of SGS TKE. CRMs dissipate TKE too efficiently due to the under-prediction of turbulence length scale, which enters the denominator of the TKE dissipation term. Bogenschutz and Krueger (2013) proposed a novel length scale formulation where sub-cloud and cloud layers are treated separately. Individual treatment of the cloud layer addresses address the issue of the commonly small in-cloud length scale values predicted by other schemes. Separate formulations can be interpreted as a reflection of the fact that sub-cloud and in-cloud circulations can become decoupled. Both formulations are non-local, allowing the capture of the sizes of the largest eddies in a given column, and both are weighted by SGS TKE strength, reflecting the fact that with grid size increase (decrease) SGS TKE on average becomes larger (smaller), accompanied by the corresponding increase (decrease) of the turbulence length scale. The new formulation was validated against high resolution LES data up-scaled to a CRM resolution, and in CRM runs with up to 25 km horizontal resolution for a variety of cloud regimes. Prognosed SGS TKE values are used to diagnose turbulent diffusion coefficients that are supplied to the host model's diffusion equation solver, and are utilized in the calculation of higher order moments of SGS PDF by the downgradient diffusion method.

SHOC is a scale-aware parameterization by virtue of the fact that with increasing resolution prognosed SGS TKE values decrease along with the magnitudes of diagnosed diffusion coefficients, leading to a decrease in the values of diagnosed higher order moments (e.g., variances) of the SGS PDF, until at the limit of infinitesimal grid size the SGS PDF collapses into a delta function in each variable with amplitude determined by the variable's grid mean value. SHOC replaces the boundary layer,

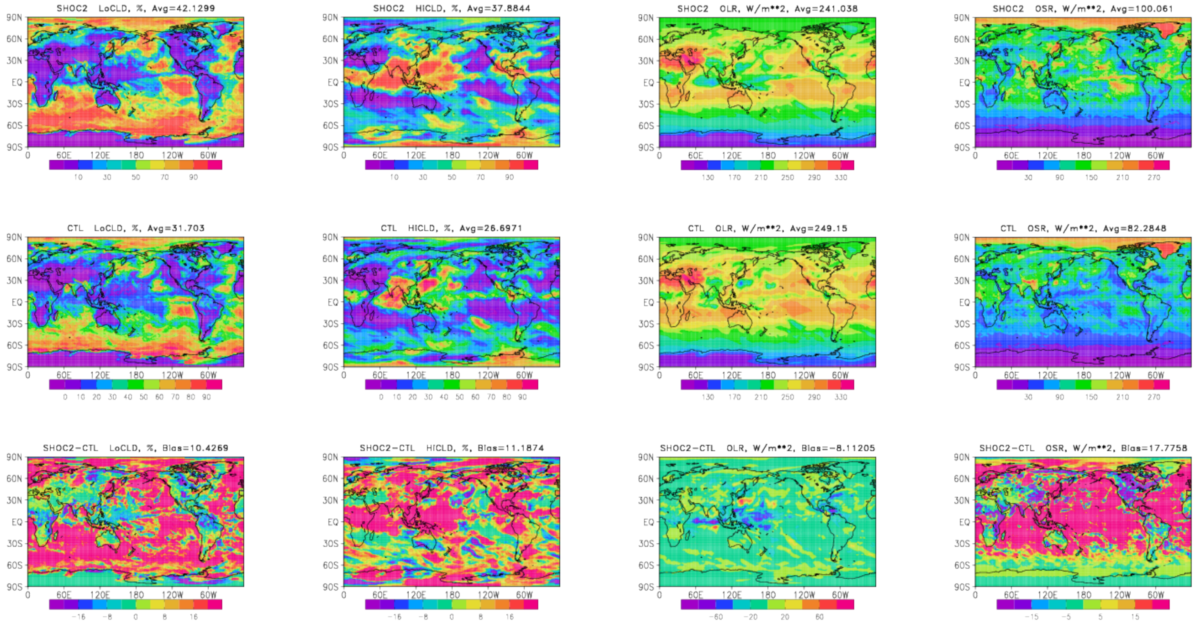

(a) Low cloud fraction, % (b) High cloud fraction, % (c) OLR, W/m^2 (d) OSR, W/m^2

Figure 1: SHOC vs control, Zhao-Carr MP, averaged over days 3-10 of a C96 forecast initialized on 8/1/17.

shallow convection, and cloud macrophysics parameterizations in a host model in a unified and self-consistent manner. As a result, the host model's cloud microphysics scheme is applied to both stratiform and shallow convective clouds, as opposed to stratiform clouds only, further unifying the representation of cloud processes.

3 SHOC Implementation in FV3 GFS

To introduce a tighter coupling between the parameterization of deep convection and the SGS cloud scheme, we replaced the diagnostic treatment of $\overline{\theta_l'^2}$, $\overline{q_t'^2}$ with prognostic equations for both moments with added source terms for the variances from deep convective detrainment following Klein et al. (2005), leading to an improvement in the simulation of upper tropospheric tropical cloudiness. Currently, only the Chikira-Sugiyama deep convection parameterization with Arakawa-Wu extension is coupled to SHOC in this manner.

A number of assumptions originally imposed on the analytical form of ADG1 were substantially relaxed, and additional damping was introduced in grid boxes with excessive diagnosed skewness of w, resulting in a better representation of stratocumulus.

The cloud macrophysics scheme was re-formulated following Firl (2013).

Fluxes $\overline{w'\theta_l'}$ and $\overline{w'q_t'}$ are now computed from the tendencies of temperature and total cloud condesate due to diffusion calculated in the diffusion subroutine by the tridiagonal matrix solver, improving the coupling to surface processes.

To account for grid variability in the vertical, interpolation from the layer centers to layer interfaces in SHOC now uses a monotone piecewise cubic Hermite interpolant. There were a number of other improvements and bug fixes.

Figure 1 shows the averages over days 3-10 of 10-day forecasts initialized on 08/01/17 at C96L64 resolution (~ 100 *km* horizontal grid size) produced by the current pre-operational FV3 GFS (control) and the same model using SHOC with the modifications listed above. Both runs use Zhao-Carr microphysics.

References

Bogenschutz, P. A. and S. K. Krueger: 2013, A simplified pdf parameterization of subgrid-scale clouds and turbulence for cloud-resolving models. *Journal of Advances in Modeling Earth Systems*, **5**, 195–211.

Bogenschutz, P. A., S. K. Krueger, and M. Khairoutdinov: 2010, Assumed probability density functions for shallow and deep convection. *Journal of Advances in Modeling Earth Systems*, **2**.

Canuto, V. M., Y. Cheng, and A. Howard: 2001, New third-order moments for the convective boundary layer. *Journal of the Atmospheric Sciences*, **58**, 1169–1172.

Cheng, A., K.-M. Xu, and B. Stevens: 2010, Effects of resolution on the simulation of boundary-layer clouds and the partition of kinetic energy to subgrid scales. *Journal of Advances in Modeling Earth Systems*, **2**.

Firl, G. J.: 2013, A study of low cloud climate feedbacks using a generalized higher-order closure subgrid model. Dissertation, Colorado State University, Ft. Collins, CO, USA.

Klein, S. A., R. Pincus, C. Hannay, and K.-M. Xu: 2005, How might a statistical cloud scheme be coupled to a mass-flux convection scheme? *Journal of Geophysical Research: Atmospheres*, **110**.

Larson, V. E., J.-C. Golaz, and W. R. Cotton: 2002, Small-scale and mesoscale variability in cloudy boundary layers: Joint probability density functions. *Journal of the Atmospheric Sciences*, **59**, 3519–3539.

A new way to compute the energy budget in GCMs and NWP models with the use of the enthalpy flux: the EBEX-2000 campaign.

by Pascal Marquet

Météo-France. CNRM/GMAP. Toulouse. France. *E-mail: pascal.marquet@meteo.fr*

1) Motivations - Introduction.

The surface energy budget is computed in GCM and NWP models by making the sum of net radiation (R_n), ground (G), sensible (H) and latent heat ($L\,.\,E$) fluxes, where E is the flux of evaporation ($\rho\,\overline{w'q'_v}$) and $L = L_v$ or L_s are the latent heat of vaporization or sublimation, depending on $T < T_0$ or $T > T_0 = 273.15$ K.

However, it is shown in Montgomery (1948), Businger (1982) and Marquet (2015b) that the flux of energy is equal to the flux of enthalpy $\rho\,\overline{w'h'}$, which is the sum of $c_p\,\overline{w'T'}$ and $L_h\,\overline{w'q'_v}$ (plus other terms if liquid water or ice exist, which are not studied here). If the first term represents the sensible flux, with c_p equal to the moist-air specific heat (at constant pressure), the difference in enthalpy of dry air and water vapour $L_h = h_v - h_d$ is different from both L_v and L_s. This result prevents $L_h\,\overline{w'q'_v}$ to represent the usual latent heat flux considered in GCM and NWP models.

The third-law definitions of the specific enthalpy h and L_h (Marquet 2015a,b) were used in Marquet *et al.* (2018) to study the energy balance closure problem (Foken, 2008) for the Météopole-Flux (MF) dataset. However, the lack of evaluation of G prevented this MF closure to be accurate with either L_v or L_h.

In the present study, the EBEX-2000 dataset (Oncley *et al.*, 2007) is used to study more realistic and relevant energy balance closure.

2) The present EBEX-2000 budget.

All terms of the energy budget are plotted in Fig.1 for the EBEX-2000 dataset. They are computed for an average over the 41 days and the 9 stations of the campaign. The fluxes are measures at 4.7 m above the ground, which is far above the height of about 1 m for the canopy of the cotton field, which is uniform over the 300×1200 m^2 area where the 9 measurements sites were placed. This leads to very good conditions for studying the energy balance closure problem.

The residual $Res = R_n - G - H - L_v.E$ is larger than 60 W/m^2 to 70 W/m^2 for daytime conditions, with a daily mean value of +21.3 W/m^2. These large values are typical of observed imbalance of energy closure, although all the "major" correction terms are taken into account (water on sonic anemometer ; Webb and Oxygen correction on hygrometer ; spatial separation of hygrometer and anenometer ; storage of energy by

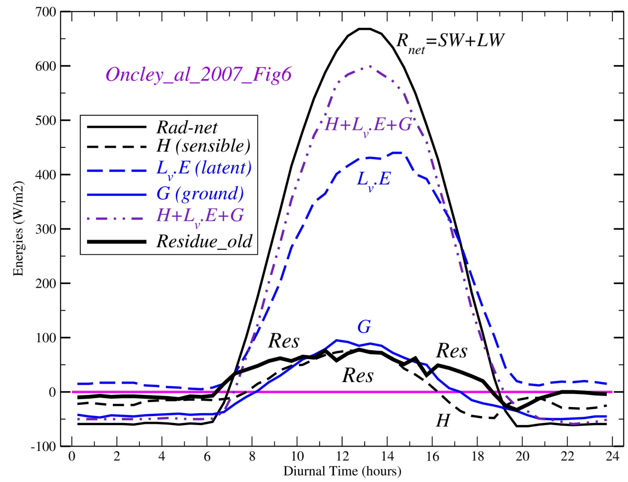

Figure 1: *The EBEX-2000 budget with the latent heat $L_v.E$.*

soil, vegetation and air added in G).

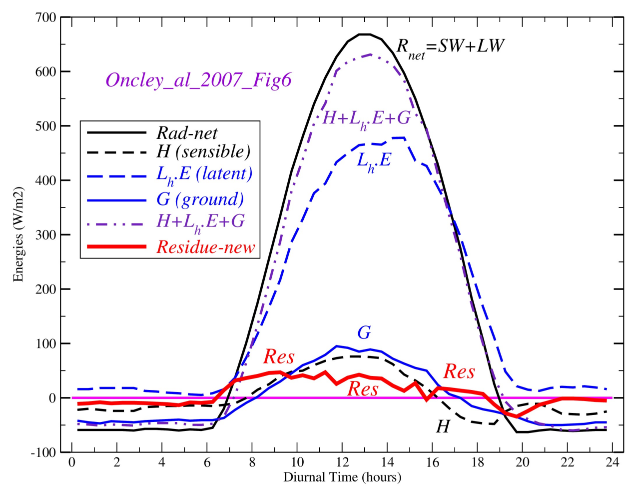

Figure 2: *The EBEX-2000 budget with the latent heat $L_h.E$.*

There is a clear diurnal cycle for all terms. This means that a possible source of imbalance (Res) could be due to any of the energy fluxes R_n, $L_v.E$, H or G. Crude evaluations (Marquet 2015b, *et al.* 2018) show that $L_h(T)$ is about +8 % larger than $L_v(T)$ for $T \approx 300$ K, where the latent heats are computed as

$$L_v(T) \approx 2501 + (c_{pv} - c_l)\,(T - T_0)\,, \quad \text{(in kJ/kg)}$$
$$L_h(T) \approx 2603 + (c_{pv} - c_{pd})\,(T - T_0)\,, \quad \text{(in kJ/kg)}$$

where $c_{pv} - c_l \approx -2.37$ kJ/kg, $c_{pv} - c_{pd} \approx +0.84$ kJ/kg, and $L_h(T_0) = 2603$ kJ/kg is given by applying a third-law hypothesis at 0 K for solid states of all species of the moist atmosphere (N_2, O_2, Ar, CO_2, H_2O).

If $L_v.E \approx 400$ W/m^2 is replaced by $L_h.E$, an increase of the turbulent fluxes by +8 % corresponds to

+32 W/m^2 at midday). This is about half of Res and it is thus relevant to test if the use of the flux $L_h.E$ may lead to more relevant energy closure.

3) The new EBEX-2000 budget.

The new budget of energy computed with $L_h(T) = h_v(T) - h_d(T)$ is plotted in Fig.2. Comparisons of the residues are facilitated in the zoomed Fig.3. The new residue (in red) is much smaller than with $L_v(T) = h_v(T) - h_l(T)$. The diurnal cycle is removed, with a decrease from 9 h to 18 h from +40 to +10 W/m^2.

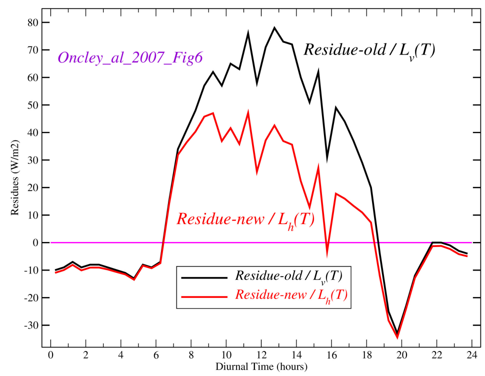

Figure 3: *The residuals with major correction terms computed with the latent heat fluxes $L_v.E$ or $L_h.E$.*

The impact of $L_h(T)$ on Res reaches -39 W/m^2 at 15 h. The new (41 days and 9 sites) daily average of the residue is close to +8.7 W/m^2 and is reduced by 12.6 W/m^2, or 59 %. The imbalance in budget energy is thus largely reduced if the flux of enthalpy is computed with the sum $\rho\, c_p\, \overline{w'T'} + \rho\, L_h\, \overline{w'q'_v}$.

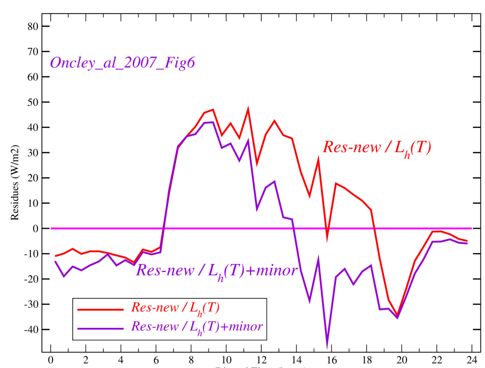

Figure 4: *The new residuals computed with L_h and with both the major and the minor correction terms.*

The residues shown in Fig.4 are computed by adding the "minor" corrections due to vertical divergence (departure from "constant fluxes" hypothesis), horizontal divergence (advection) and photosynthesis (by plants).

The daily averages for the 41 days and 9 sites mean values (with "major+minor" corrections) are +9.1 W/m^2 with $L_v(T)$ and -3.5 W/m^2 with $L_h(T)$. The imbalance in budget energy computed with $L_h(T)$ and the new flux of enthalpy is thus close to equilibrium and becomes negative. Moreover, the residue becomes smaller than ± 40 W/m^2, with positive value in the morning and negative values in the evening. These new patterns look like true residual errors.

4) Conclusions.

It is shown that the budget of energy of EBEX-2000 can be nearly balanced in (time and sites) average if the sum of "sensible" and "latent" heats are replaced by the flux of enthalpy $\rho\,\overline{w'h'} = \rho\, c_p\, \overline{w'T'} + \rho\, L_h\, \overline{w'q'_v}$.

Differently, the equations for temperature dT/dt at the surface and in the atmosphere must still involve the usual definition of "sensible" and "latent" heat fluxes $\rho\, c_p\, \overline{w'T'} + \rho\, L_v\, \overline{w'q'_v}$ (or $\rho\, L_s\, \overline{w'q'_v}$ over icy surface).

This complex situation can be understood because we use both of the two equivalent equations:

$$\frac{dh}{dt} = A = (\ldots) - \frac{1}{\rho}\, \vec{\nabla}.\left(h_k\, \vec{J}_k\right) \quad \text{and}$$

$$\frac{d(c_p T + L_v^0\, q_v)}{dt} = B = (\ldots) - \frac{1}{\rho}\, \vec{\nabla}.\left(L_v^0\, \vec{J}_v + c_{pk}\, T\, \vec{J}_k\right),$$

where $L_v^0 = L_v(0\,\mathrm{K})$, $\vec{J}_k$ are the diffusion fluxes and the implicit sums $h_k\, \vec{J}_k$ and $c_{pk}\, \vec{J}_k$ are for dry air and water vapour (this note is for clear air with $q_l = q_i = 0$).

These equations are fully equivalent, but $A \neq B$ because the left and right hand sides are not the same due to $h \neq c_p T + L_v^0\, q_v$. Therefore, it is not possible to close at the same time the budget for the energy ($A = 0$ with the use of L_h) and for the Moist Static Energy $c_p T + L_v^0\, q_v$ ($B = 0$ with the use of L_v). The way the budget of energy is computed in GCMs and NWP models must be improved by relying on general thermodynamics and by using $L_h = h_v - h_d$ (not L_v).

References

• Businger J. A. (1982). The fluxes of specific enthalpy, sensible heat and latent heat near the Earth's surface. *J. Atmos. Sci.* **39**: p.1889–1892.

• Foken T. (2008). The energy balance closure problem: An overview. *Ecological Appl.* **18**: p.1351–1367.

• Marquet P. (2015a). On the computation of moist-air specific thermal enthalpy. *Q. J. R. Meteorol. Soc.* **141**: p.67–84. `https://arxiv.org/abs/1401.3125`

• Marquet P. (2015b). Definition of Total Energy budget equation in terms of moist-air Enthalpy surface flux. *CAS/JSC WGNE*. WCRP Report No.12, `http://bluebook.meteoinfo.ru/`

• Marquet P., Canut G., Maurel W. (2018). An evaluation of the energy budget computed with observed enthalpy surface fluxes. *CAS/JSC WGNE*. WCRP Report No.15, `http://bluebook.meteoinfo.ru/`

• Montgomery R. B. (1948). Vertical eddy flux of heat in the atmosphere. *J. Meteorol.* **5**: p.265–274.

• Oncley S.P., Foken T. *et al.* (2007). The Energy Balance Experiment EBEX-2000. Part I: overview and energy balance. *Bound.-Layer Meteor.* **123**: p.1–28. *Thanks to UCAR/NCAR-Earth Observing Laboratory.*

A new “grid-point storm control” scheme in the ARPEGE NWP model

by Pascal Marquet, Laurent Descamps, François Bouyssel

Météo-France. CNRM/GMAP. Toulouse. France. *E-mail: pascal.marquet@meteo.fr*

1) Motivations - Introduction

It is explained in Bechtold (2008) that spurious grid-point storms can be generated in NWP models when convective heating/mixing (stabilisation) is not adequately represented (with too weak convection and/or turbulent schemes). The model can then become saturated under moist and/or strong forcing conditions, and an explicit turnover can develop to get rid of the instability.

(a) (b)

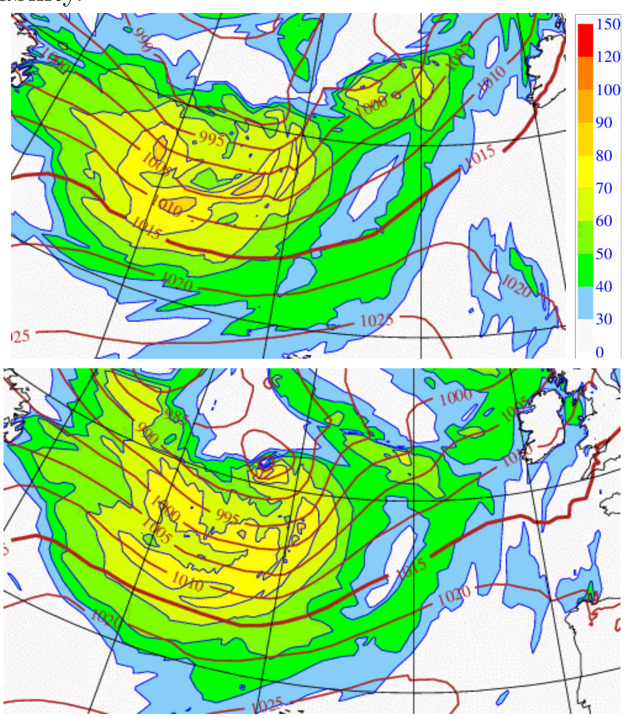

Figure 1: *Outputs of ARPEGE for the “low-resolution” operational version (T1198 / c = 2.2). The mean sea level pressure (MSLP, contours every 5 hPa) and 10 m wind speed (color scale, km/h) are plotted with the operational GPSC scheme for: (a) the analysis for the 11th of March 2017 (00 UTC) ; and (b) the 72 h forecast (from the 8th of March). The coasts from Ireland to Portugal are located on the right in (b).*

These unphysical strong ascents in the model are called “grid-point storm” (GPS). They can produce excessive large-scale rain, too deep lower tropospheric pressure systems and strong divergence at upper levels. They can destroy the actual Jet structure, and the model error can propagate and grow quickly, affecting heavily the forecast skill and the readability of the model synoptic charts.

An example of such a GPS is shown in Fig.1(b): there is a small region in the mid/north Atlantic where the isobaric lines are too close to each other (especially on the SW side of the low-pressure system) and generate too strong low-level winds (> 80 km/h). These patterns do not exist in the analysis chart in (a).

However, a curative scheme is active in the operational version of the French ARPEGE model. The current “grid-point storm control” scheme (GPSC) is implemented in the Bougeault convective scheme (1985), based on the convective equations of Yanai *et al.* (1973):

$$\left(\frac{\partial s}{\partial t}\right)_{\text{conv.}} = \omega^* \, \frac{\partial s}{\partial p} + K \, (s_c - s) - g \, \frac{\partial F_s}{\partial p} \, , \qquad (1)$$

$$\left(\frac{\partial q_v}{\partial t}\right)_{\text{conv.}} = \omega^* \, \frac{\partial q_v}{\partial p} + K \, (q_c - q_v) - g \, \frac{\partial F_q}{\partial p} \, . \qquad (2)$$

The turbulent fluxes F_s and F_q are removed from (1)-(2) for $s = c_p T + \phi$ and q_v so that the convection scheme might be aware of how the turbulence will modify the vertical profile (Bougeault, 1985). The mass flux ω^* is a measure of the net vertical ascent for the cloud profile values (s_c, q_c). The detrainment coefficient K is deduced from the conservation of moist static energy $\text{MSE} = s + L_v \, q_v$ along each vertical column.

Similarly to what is done with the removal of the turbulent fluxes F_s and F_q in (1)-(2), the GPSC scheme is based on a removal of the impact of the moisture convergence $\text{MCVG} = -\,\omega^* \partial q_v / \partial p$ for each levels and where the resolved vertical velocity is large ($|\omega| > \omega_0 \approx 1$ Pa/s). The impacts of the MCVG are thus added to the diffusion fluxes F_s and/or F_q. Moreover, the GPSC scheme is limited to moist regions where $\text{RH} = 100 \; (q_v / q_{sat}) \; > 100$ %. It is expected that the knowledge of possible moist-saturated regions with high values of ω can enhance the action of the mass-flux scheme, with a possible removing of the observed spurious grid-point storms in ARPEGE.

A long trials and errors process showed (Bouyssel, 2012, in French) that an efficient method was to add the impact on the flux of static energy F_s only. However, some unexpected and unrealistic (dry-air) tropical waves were generated by this method. For this reason, the present version of the GPSC scheme only modifies the turbulent flux of specific humidity F_q.

2) Impacts of the higher resolution

An increase in resolution of ARPEGE is scheduled in 2019 by a factor 1798/1198 = 1.50 (thus by +50 %). Since the size of the finest resolved scales become 50 % smaller, the grid-point storm (GPS) must likely become more frequent and/or intense. A counting by eyes confirmed this risk over a period of 5 months: 18 GPS with the low resolution, versus 23 GPS for the high resolution.

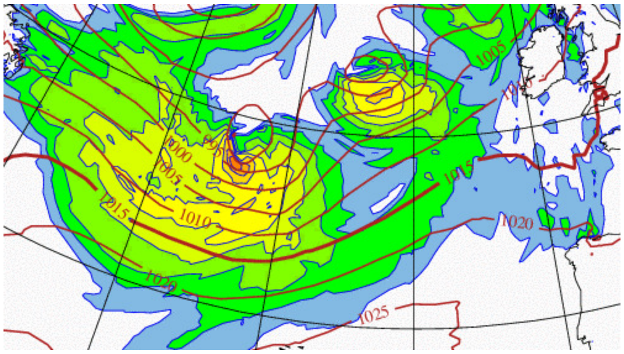

Figure 2: *The same 72 h forecast as in Fig.1(b), but for the new "high-resolution" in test (T1798 / c = 2.2).*

A typical example of such a new GPS generated by the high resolution is shown in Fig.2 (mid-Atlantic). A comparison with the Fig.1(b) shows that the GPS generates stronger low-level winds (> 100 km/h) than with the same GPSC scheme at low-resolution. Moreover the isobaric lines of MSLP are clearly asymmetric.

A test experiment made on the same day as in Fig.2 confirms that if the operational GPSC scheme is switch-off, then more GPS appear and generate frequent "bubbles" along the cold-front (see Fig.3).

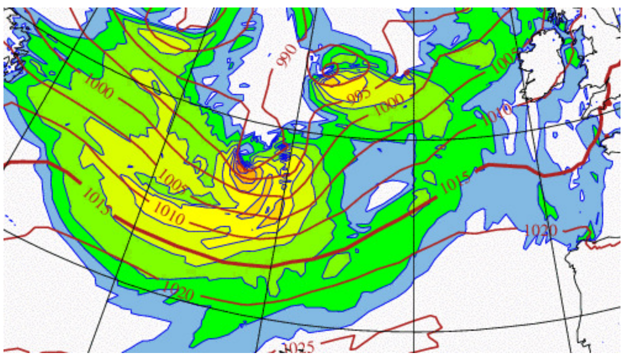

Figure 3: *The same as in Fig.2, but without any GPSC scheme. Two new GPS are observed, with enhanced winds, too.*

3) Impacts of the new scheme

The new GPSC scheme tested in 2018 corresponds to a removal of the impact of the moisture convergence MCVG via the turbulent fluxes of static energy F_s. Moreover, the threshold of 100 % for RH is now variable: it is imposed in the tropical region (in order to remove the spurious dry-air waves), whereas it is closer to 70 % for the extra-tropical cyclones (see Fig.4).

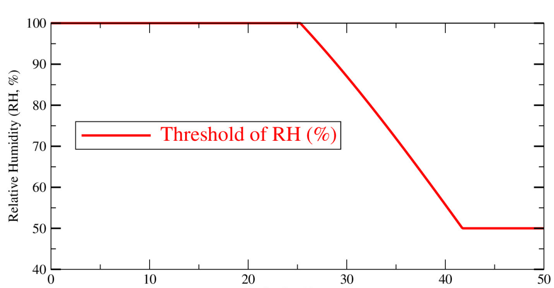

Figure 4: *The threshold of RH in terms of the latitude.*

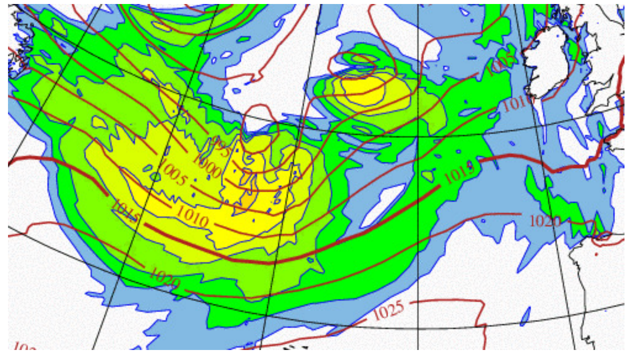

Figure 5: *The same "high-resolution" 72 h forecast as in Fig.2, but with the new GPSC scheme.*

The impact of this new scheme is shown in Fig.5. A comparison with Fig.2 shows that the grid-point storm is removed, with more realistic features for both the MSLP (more symmetric isobaric lines) and the 10 m wind speed (< 85 km/h). Moreover, the spurious tropical waves observed in 2012 are removed (not shown) by protecting the tropical region from the action of the new GPSC scheme via the threshold for RH. This new GPSC scheme is implemented in the test-suite in 2018 for a possible operational used in 2019.

4) Conclusions

It was necessary to improve the operational GPSC scheme for preparing the high resolution of ARPEGE (T1798 / c = 2.2). It seems that the new GPSC scheme leads to some improvements of some scores (to be confirmed, not shown).

However, the best solution to get rid of the spurious GPS in ARPEGE would be to improve the deep convection scheme itself. This has been confirmed by a test of the IFS scheme (Tiedtke 1989, Bechtold *et al.* 2014) in ARPEGE, with no more than 3 grid-point storms observed over the same period of 5 months (instead of 23).

References

• Bechtold P. (2008). *Numerical weather prediction parameterization of diabatic processes. Convection IV: forcasting and diagnostics.* ECMWF NWP training course.

• Bechtold, P. *et al.* (2014). Representing equilibrium and non-equilibrium convection in large-scale models. *J. Atmos. Sci.* **71**: 734–753

• Bouyssel F. (2012). *Note de synthèse sur les modifications "anti-arpeageades" introduites dans le schéma de convection profonde dans les modèles Apege et Aladin.* Météo-France/CNRM/GMAP internal report.

• Bougeault P. (1985). A simple parameterization of the large-scale effects of cumulus convection. *Mon. Wea. Rev.* **113**: 2108–2121.

• Tiedtke, M. (1989). A comprehensive mass flux scheme for cumulus parameterization in large-scale models. *Mon. Wea. Rev.* **117**: 1779-1800.

• Yanai M., Esbensen S., Chu J.-H. (1973). Determination of bulk properties of tropical cloud clusters from large-scale heat and moisture budgets. *J. Atm. Sci.* **30**: 611–627.